Journal of Power Sources 356 (2017) 356–364

Contents lists available at ScienceDirect

Journal of Power Sources

journal homepage: www.elsevier.com/locate/jpowsour

Energy harvesting influences electrochemical performance of microbial fuel cells

Fernanda Leite Lobo [a], Xin Wang [b], Zhiyong Jason Ren [a, *]

[a] Department of Civil, Environmental, and Architectural Engineering, University of Colorado Boulder, Boulder, CO, 80309, USA
[b] MOE Key Laboratory of Pollution Processes and Environmental Criteria / Tianjin Engineering Center of Environmental Diagnosis and Contamination Remediation, Nankai University, Tianjin, 300350, China

HIGHLIGHTS

- Demonstrates for the first time how active harvesting affects MFCs.
- Harvesting significantly improves performance in all operation points.
- Different goals lead to different operation strategies.

GRAPHICAL ABSTRACT

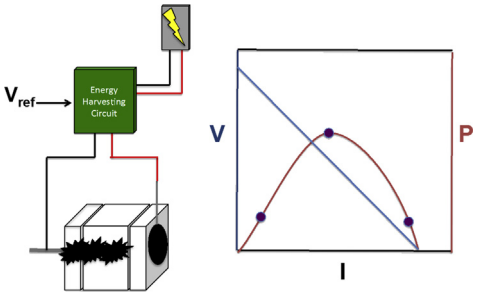

ARTICLE INFO

Article history:
Received 10 December 2016
Received in revised form
15 March 2017
Accepted 16 March 2017
Available online 22 March 2017

Keywords:
Microbial fuel cell
Maximum power point
Maximum current point
Energy harvesting
Wastewater

ABSTRACT

Microbial fuel cells (MFCs) can be effective power sources for remote sensing, wastewater treatment and environmental remediation, but their performance needs significant improvement. This study systematically analyzes how active harvesting using electrical circuits increased MFC system outputs as compared to passive resistors not only in the traditional maximal power point (MPP) but also in other desired operating points such as the maximum current point (MCP) and the maximum voltage point (MVP). Results show that active harvesting in MPP increased power output by 81–375% and active harvesting in MCP increased Coulombic efficiency by 207–805% compared with resisters operated at the same points. The cyclic voltammograms revealed redox potential shifts and supported the performance data. The findings demonstrate that active harvesting is a very effective approach to improve MFC performance across different operating points.

1. Introduction

Microbial fuel cells (MFCs) employ electroactive bacteria to produce direct electrical current from biodegradable substrates and demonstrate great potentials for energy-positive wastewater treatment, remote sensing, and environmental remediation [1–5]. Despite great advancements on reactor configurations, materials, and operations, the power density of a single MFC reactor still ranges between mW m^{-2} and W m^{-2}, which is not enough for real-world applications [6]. Higher power may be obtained by connecting multiple MFCs in series or parallel, but the operation is challenging and performance is unstable due to voltage reversal and other problems associated with the non-linear nature of biological systems [7–11].

* Corresponding author.
E-mail address: zhiyong.ren@colorado.edu (Z.J. Ren).

http://dx.doi.org/10.1016/j.jpowsour.2017.03.067
0378-7753/

Maximum power point (MPP) tracking and power management systems (PMS) have been used for MFC research and development, and reported methods include perturbation and observation [12], multiunit monolithic system [13,14], hysteresis controller, synchronous flyback converter, and transformer [8,9,15,16]. Many of these methods reported improved power production especially when using pulsed active energy harvesting approach because they are able to provide real-time energy tracking and capturing and therefore maximize power output. For example, Wang et al. reported that hysteresis controller based MPP circuit was able to harvest 76 times more energy than a charge pump and increase Coulombic Efficiency by 21 times [16]. New integrated circuits and chips significantly reduced volume and energy consumption of the controller and therefore increased energy harvesting efficiency and enabled self-sustaining operation [5,14]. However, MPP may not be the best operating point for all applications. For fuel and chemical productions from microbial electrolysis cells or water desalination from microbial desalination cells, maximum current point (MCP) is generally preferred because higher current can drive faster chemical production or ion separation (Fig. 1) [6,17,18]. For MFCs used in wastewater treatment, the primary goal may not be high power output either depending on operation stages, because for efficient organic removal higher current is desired. Therefore, in reality a balance in operation needs to be considered whether to operate the system at the MPP for maximum power output or at the MCP for faster substrate oxidation.

To our best knowledge no study has investigated how active harvesting at different regions (high power, high current, or high voltage) affects MFC electrochemical performance and substrate conversion efficiency, and very limited information is available on comparing system performance under active harvesting or traditional resister-based operation. Previous studies showed that passive loads did impact the anode biofilm thickness and community structure by influencing the anode potential [19,20], but the electrochemical performance such as power production could maintain stable once biofilm reached to a level of electron transfer capability. In contrast, the pulse-shaped power extraction uses power electronic converters with high frequency therefore could lead to swifts in microbial electron transfer processes and anode biofilm change [6]. In this study, we investigated extensively how different energy harvesting scenarios including both active harvesting and passive resistor loads affect MFC electrochemical performance and associated microbial activities. System behavior at three operating points including high power, high current, and high voltage were analyzed in different harvesting conditions, and the implications of how harvesting affect MFC operation are discussed.

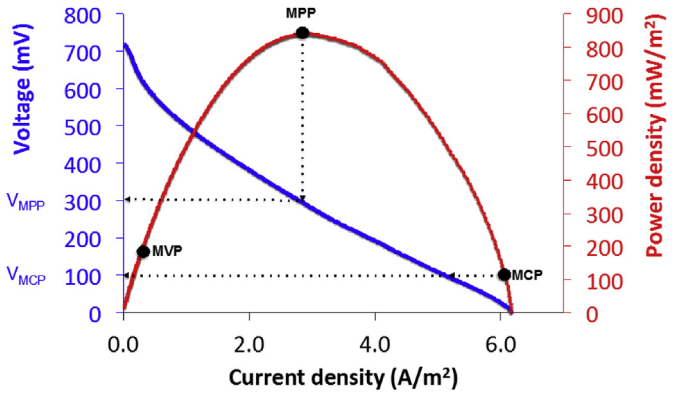

Fig. 1. The power density curve obtained in an MFC operated under a 1000 Ω external resistance. This curve shows the typical Stage I operation and was used to determine different operational points (MPP, MCP, MVP).

2. Materials and methods

2.1. MFC construction and operation in two stages

Cubic single-chamber MFCs were constructed using polycarbonate, and the empty volume of the MFC chamber was 28 mL. Each MFC reactor contained a heat-treated graphite brush as the anode and a carbon cloth air-cathode (7 cm^2, Fuel Cell Earth) with manufacturing procedure described in previous studies [21,22]. Diluted brewery wastewater from Avery Brewery (Boulder, CO) was used as the sole substrate during the experiment, and 50 mM phosphate buffer solution (PBS, $NaH_2PO_4 \cdot 2H_2O$ 3.32 g L^{-1}; $Na_2HPO_4 \cdot 12H_2O$ 10.32 g L^{-1}; NH_4Cl 0.31 g L^{-1}; KCl 0.13 g L^{-1}) was used for the 1:10 dilution [23]. The final substrate electrolyte used in the study contained 1800 mgL^{-1} COD, 938 mgL^{-1} TKN, and 1860 mgL^{-1} PO_4^{3-}. All MFCs were run in duplicate in batch mode at room temperature, and fresh medium was refilled at the end of each batch cycle.

The experiment was divided in two stages. In stage I, all 10 reactors were operated under the same condition with an external resistance of 1000 Ω. This stage lasted for 2 months until similar performance was obtained which indicate the establishment of a baseline for further research. Using the power density curves derived from linear sweeping voltammetry (LSV) from each MFC reactor at the end of stage I, the key operating points of maximum current points (MCP), maximum voltage points (MVP) and maximum power points (MPP) were identified for phase II operation. In phase II, the reactors were divided in 5 groups. Each group has duplicate reactors and was operated in one of the following scenarios: maximum power with active energy harvesting (MPP-H), maximum current with active energy harvesting (MCP-H), maximum power with passive resistor (MPP-R), maximum current with passive resistor (MCP-R), and maximum voltage with passive resistor (MVP-R) (Fig. 1).

For the passive energy harvesting conditions, the operating resistors were determined by dividing voltage with current at desired points on the power density curve. Specifically, the external resistors used in MVP-R, MPP-R, and MCP-R scenarios were 2.2 kΩ, 150 Ω, and 33 Ω, respectively. For active harvesting scenarios, MPP-H and MCP-H circuits were controlled by operating voltages that were determined during phase I operation (Fig. 1).

The energy circuit used in this study was the bq25505 (Texas Instruments Inc.), which is an integrated energy harvesting Nano-Power management circuit, specifically designed to efficiently acquire and manage the microwatts (μW) to milliwatts (mW) of power generated from a variety of high output impedance (Hi-Z) DC sources with a highly efficient, pulse-frequency modulated (PFM) boost converter/charger. Embedded in the integrated circuit, a programmable maximum power point tracking (MPPT) keeps sampling the open circuit input voltage every 16 s by disabling the boost converter for 256 ms and stores the programmed MPP ratio of the open circuit voltage on the external reference capacitor at VREF_SAMP. In this study, we adjusted the programmable MPPT to set VREF-SAMP to be at either V_{MPP} = 300 mV (MPP-H) or V_{MCP} = 100 mV (MCP-H) showed in Fig. 1, and this control was able to maintain a constant MFC voltage. Since the maximum current would be given at 0 V, the approximation of V_{MCP} = 100 mV was used to give highest current controlled possible by the energy harvester circuit. The energy extracted from each MFC was stored in polymer lithium ion batteries (840 mAh, SparkFun Electronics®).

2.2. Analyses

The individual potential of each anode and cathode was measured each batch using Ag/AgCl reference electrodes (RE-

5B, +0.210 V versus standard hydrogen electrode, 25 °C). Reactor voltages were recorded using a data acquisition system (Keithley, OH). Cyclic voltammetry (CV) was performed before and after batch operations in different stages. The potential range for CV was determined as −0.7 to 0 V vs. Ag/AgCl according to previous results and the scan rate was 1 mVs^{-1} [24]. First derivative CV (DCV) was derived from turnover CV to determine the changes in each peak value. The main oxidation peak in DCV was fitted to Guassian function to separate overlapped peaks. LSV tests were performed using the same potentiostat with a scan rate of 1 mVs^{-1} with either the anode or the cathode as the working electrode depending on characterization purposes.

Chemical oxygen demand (COD) before and after each batch was measured using the standard method with a spectrophotometer (DR 3900, Hach Co., Loveland, CO, USA). Coulombic efficiency was determined using Equation (1), where $M = 32$ (molecular weight of oxygen), F is faraday constant, $b = 4$ is the number of electrons exchanged per mole of oxygen, v_{an} is the liquid volume of anode compartment, and ΔCOD is the change in COD over time [25,26].

$$CE = \frac{M\int_0^t Idt}{Fbv_{an}\Delta COD} \quad (1)$$

3. Results and discussion

3.1. Variations of MFC voltage, current, and electrode potentials in different conditions

Fig. 2A–E summarizes the profiles of MFCs operated in different stages and different harvesting conditions. Similar profiles were observed across all MFCs in the first 60 days (Stage I), in which all reactors were operated in the same condition of 1000 Ω external resistor. The reactors showed typical batch cycles of 3.5 days with the maximum MFC voltage of ~430 mV, the maximum current of ~0.43 mA, the lowest anode potential of −460 mV and the maximum cathode potential of 180 mV. The maximum power density achieved ranged from 598 mW m^{-2} to 844 mW m^{-2} (average 739 mW m^{-2}) among 10 reactors.

Starting from day 61, the reactors are divided into 5 groups as aforementioned (MPP-H, MPP-R, MCP-H, MCP-R, and MVP-R), and different profiles in voltage, current, and electrode potentials are shown in Fig. 2A–E. For the reactors operated in the maximum power point, stable voltage, current, and anode and cathode potentials were generated under the MPP-H condition (Fig. 2A). This is due to the dynamic control of harvesting voltage around 300 mV by the energy harvesting circuit through pulse frequency modulation. As shown in Fig. 3A, under the active control, the MFC voltage was regulated to increase until 312 mV and decrease until 256 mV in high frequency. This harvesting approach enables real time feedback of the MFC's MPP changes during operation and adjusts harvesting condition accordingly. Since the MFC voltage was controlled to be constant, the MFC current was the one indicating the MFC batch cycle, which varied between around 1.3 mA and 0.7 mA. The MPP-H batch cycles were 24 h each in order to stay in the maximum power area of the power density curve. In contrast, the outputs from MPP-R varied significantly within each batch, with voltage changed from 20 to 280 mV and current fluctuated from 0.1 mA to 1.8 mA (Fig. 2B). While such fluctuation is commonly observed in fed-batch MFC studies, it does reduce energy output and system stability compared with circuit harvesting (Fig. 4).

For reactors operated at the maximum current point, similar trends were observed. Fig. 2C shows that the MCP-H circuit controlled MFC voltage to stable at around 100 mV, and stable anode and cathode potentials were maintained throughout the operation. The MCP-H MFC current varied between 3.0 mA and 2.0 mA in each 24-hour batch cycle. The difference in redox potentials between the anode and the cathode (100 mV) was much smaller than the MPP-H (300 mV), which is understandable considering the MFC was operated at the highest current and low voltage condition. Fig. 3B shows the MFC voltage being controlled in high frequency and varied between 132 mV and 24 mV, indicating a higher ripple than the MPP-H voltage. This is due to the high difficulty in controlling the low voltage by the nanopower harvester circuit. The MCP-R reactors started with a maximum voltage of ~30 mV but the performance dropped significantly in the following cycles in both reactors. While the anode potentials maintained normal, the air-cathode potentials dropped significantly, led to reactor failure. Cleaning and replacing the cathodes resumed current generation but the voltage output still showed high fluctuation.

The MVP-R reactor was operated at the maximum voltage point (Fig. 2E), which serves as a control reactor because such operation is not desired in practical applications due to its low current (slow organic removal) and low power output (low energy generation). The reactor showed stable performance in longer batch cycles (72 h) due to slow electron transfer. The maximum voltage obtained was 525 mV and the maximum current was 0.25 mA.

3.2. Variations of substrate utilization and energy recovery

Fig. 4 summarizes the performance of different MFCs in terms of COD removal, Coulombic efficiency, and power generation. Overall reactors with active harvesting showed superior performance than those with resistors, but the differences vary depending on the operation. As a baseline, in stage I the MFCs showed consistent COD removal of 95% ± 1%, protein removal of 90% ± 10%, coulombic efficiency of 14% and an average power 108 mW m^{-2}, and each batch cycle lasted for 3.5 days (80 h).

Because different harvesting scenarios led to various speeds of substrate conversion to currents, different durations of batch tests were conducted to characterize the degradation and energy recovery. The most efficient reactors for the conversion including MPP-H, MCP-H, and MCP-R were tested in 24-hour batch operation, and MPP-H showed higher COD removal (90%), which was 8% and 32% higher than MCP-H and MCP-R, respectively (Fig. 4A). Operated at the high power point, the MPP-H also showed much higher power generation than the other reactors (Fig. 4C). On the other hand, the MCP-H showed higher CE than MPP-H and MCP-R, which is consistent with the purpose of high current recovery in MCP operation (Fig. 4B). The performance of MCP-R fluctuated significantly as aforementioned, so the data obtained may not reflect the true potential of those reactors.

In 48-h batch tests, the results from the reactors also supported the hypothesized performance. For reactors operated at the maximum power points, both MPP-H and MPP-R showed good COD removal (95%) (Fig. 4A), which was slightly higher than MCP-H. However, because MPP-H extracted more electrons, it showed higher CE than MPP-R, which also resulted in much higher power generation (Fig. 4B and C). For MCP-H, similar as 24-hour batch test, it recovered much more electrons from COD and therefore achieved the highest CE among the reactors. While similar COD removals were observed in MPP-H and MCP-H reactors in 24-hour and 48-hour batches, the CE obtained in 48-hour operation were approximately doubled compared with the 24-hour batches. Also, compared with the performance obtained in Stage I, MPP-H operation improved CE by 47–77% (average 62%), MCP-H increased CE

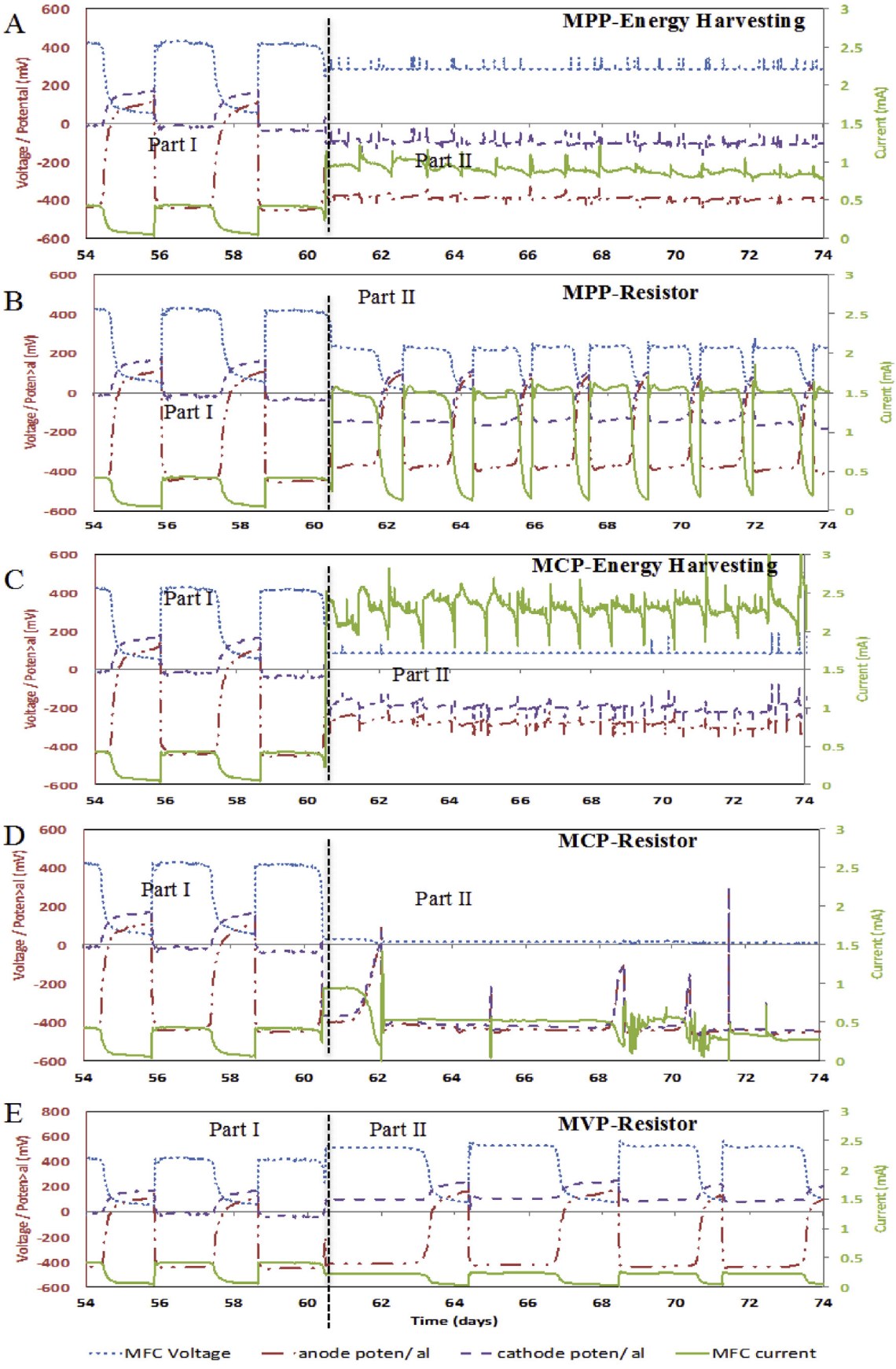

Fig. 2. Time-course profiles of MFC voltage (blue), MFC current (green), anode potential (red) and cathode potential (purple) profiles for (A) MPP-H, (B) MPP-R, (C) MCP-H, (D) MCP-R, and (E) MVP-R. (For interpretation of the references to colour in this figure legend, the reader is referred to the web version of this article.)

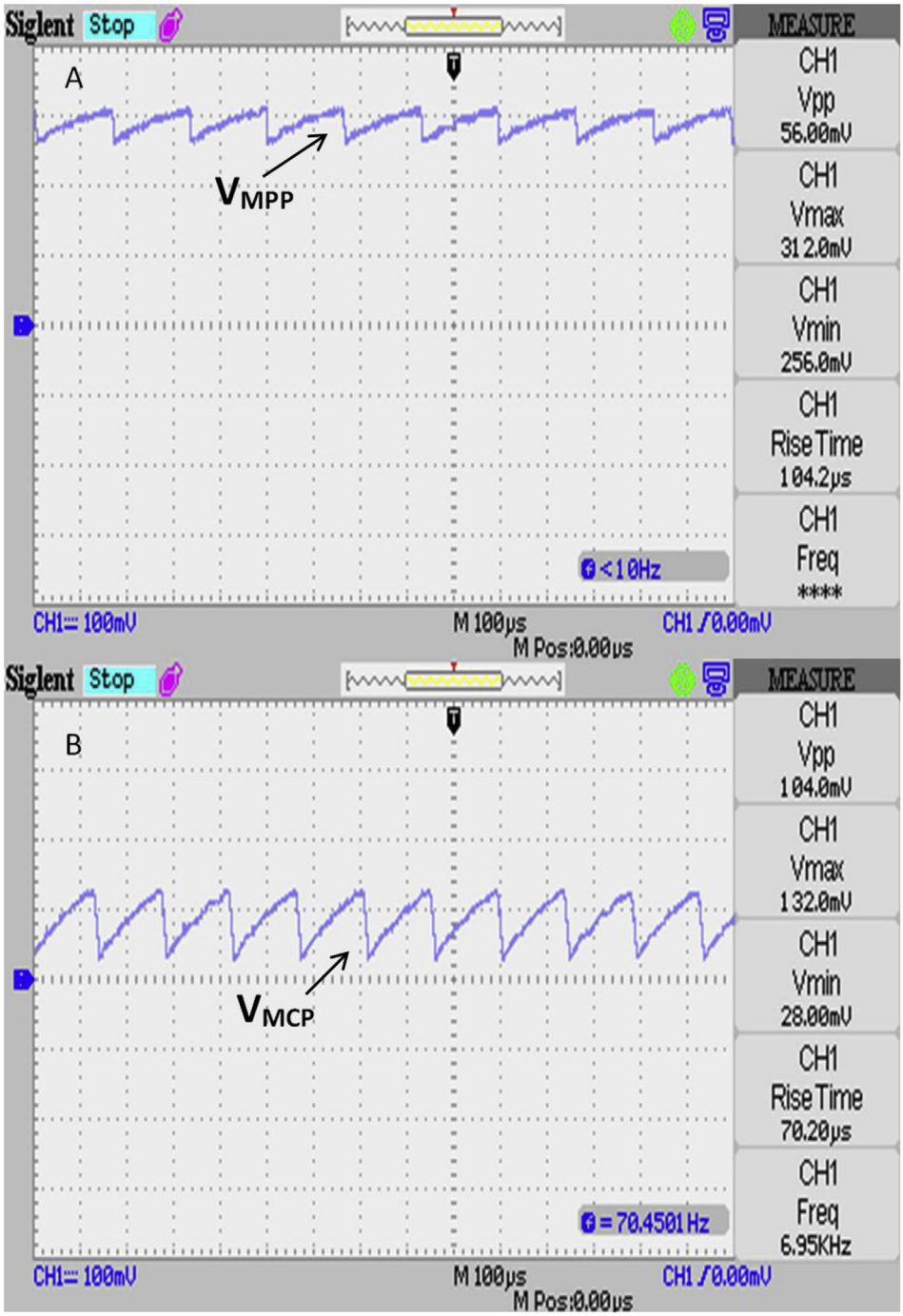

Fig. 3. The harvesting circuit controlled MFC voltages for (A) MPP-H and (B) MCP-H.

by 67–88% (average 78%), and MPP-R increased CE by 66%. The MVP-R also achieved 95% removal but it took much longer operation (72-hour cycle), and the CE and power generation was very low compared with other operations.

3.3. Redox potential shifts in cyclic voltammograms

Turnover cyclic voltammetry was performed in different stages of MFC operation to reveal the potential changes in microbial electrochemical activities [27]. Fig. 5A–E shows the temporal changes of cyclic voltammograms in each of the operation condition on day 60 (Stage I, all operated under 1000 Ω), day 90 (30 days after shifted to respective harvesting regimes in stage II), and day 114 (54 days after shifted to respective harvesting regimes in stage II).

All curves in stage I are similar with midpoint potentials at 380 ± 20 mV and currents at 3.5 ± 0.5 mA. The peaks mean the highest electron transfer rate. The duplicate reactors showed similar profiles so only one profile is shown in Fig. 5. Figs. S1–5 shows the first derivative of CVs (DCVs) for all the scenarios, which indicates more clearly the midpoint potentials. The midpoint potential on the oxidation curve indicates the redox reaction and electron transfer occurred at the anode at that potential.

When the reactors were switched to different harvesting

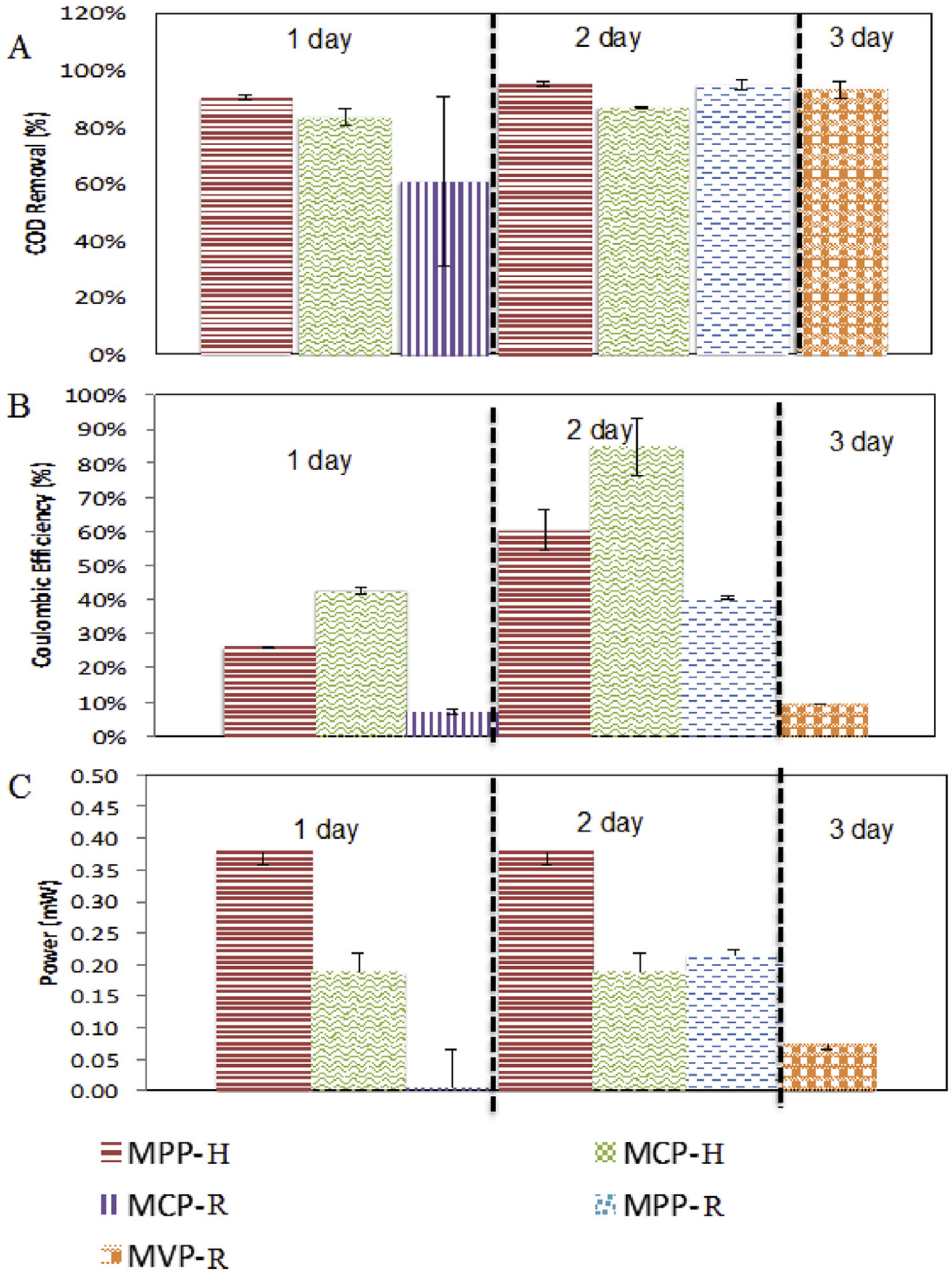

Fig. 4. (A) COD removal, (B) Coulombic Efficiency, and (C) Power Production from reactors operated in different conditions. Different durations of batch cycles were used and indicated in the graph to reflect the conversion rate differences among reactors.

regimes, the redox reaction profiles changed very differently. The MPP-H reactors showed the highest power output among all reactors, and its midpoint potential shifted negatively from −380 mV to −400 mV by day 90 and further down to −450 mV by day 114. The corresponding peak current almost tripled from increased 3.5 mA in stage I to 9.8 mA on day 90, and it further increased to 15 mA by day 114. This trend indicates a clear increase in electron transfer rate which is supported by other results as well.

Current increase was also observed in MPP-R reactors but to a lesser scale. The peak current increased from 3.2 mA to 5.5 mA, which was accompanied by the shift of midpoint potential from −380 mV to −400 mV. Interestingly, the CV profile at day 114 showed the limited current never reached a plateau, indicating a midpoint potential could not be identified. This has been reported before and was hypothesized due to the mix of electroactive cytochromes with different midpoint potentials involved in electron transfers especially in mixed culture biofilms. Other studies also suggested if the dominant species is *Shewanella*, the electron transfer may happen at the midpoint potential higher than the scan range [28]. However, it is unlikely that *Shewanella* was the dominant species in this study, because even though microbial community was not analyzed, the same inoculum was used in our recent study and *Geobacter spp.* was found to be the main electroactive bacterial species [24].

For MCP-H, higher anode midpoint oxidation potential was observed, which is consistent with reference electrode measurement. The current in Stage II was higher than stage I but not significant as compared with MPP-H. For MCP-R and MVP-R the midpoint potential shifted negatively at the beginning of stage II (from −400 mV to −450 mV), but it kept stable since after.

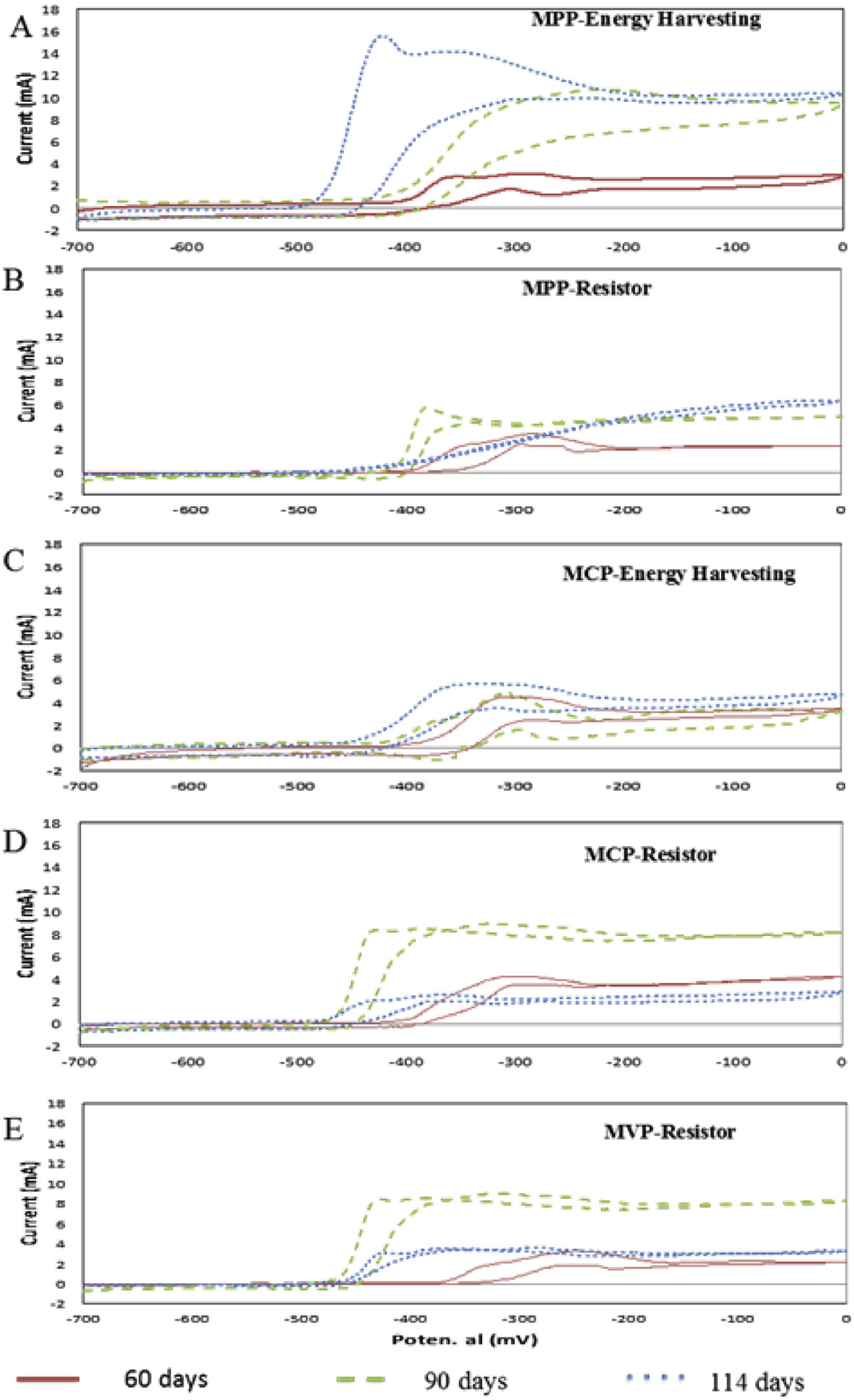

Fig. 5. Cyclic voltammetry profiles of (A) MPP-H, (B), MPP-R, (C) MCP-H, (D) MCP-R, (E) MVP-R in different stages and operational points.

However, the current decreased in both cases, indicating slower electron transfer by the biofilm. For MCP- R the CV did show higher current (8.2 mA) at a similar midpoint potential, because the resistor was changed from 1000 Ω to 33 Ω.Similar results were reported in DCVs by previous studies [29] when reactors were acclimated with high resistance but switched to lower resistance. For MVP-R, it was not clear why the initial current increased after the resistor changed from 1000 Ω to 2200 Ω, but after stabilization the end point current dropped to a similar point as the one in Stage I. The narrower and more negative midpoint potentials presented in MVP-R (2200 Ω) DCVs were also observed in DVCs in our previous study when using high external resistors (Figs. S5B and S5C) [29].

The MPP-H condition showed very high current peaks over a narrow anode potential range (−500 mV to −400 mV). This is because the anode potential in MPP-H was maintained between −400 mV and −380 mV by the harvesting circuit. Similarly, MCP-H peak was over broader and positive anode potential range (−473 mV to −330 mV) than MPP-H, with the circuit controlling the anode potential between −220 mV and −340 mV. These voltammogram profiles are very similar as the CV graphs shown by Commault, et al., [30] when they fixed the anode potential at −0.25 V. The control of MFC voltage via energy harvesting generates a mechanism to stabilize the redox potentials closer to the set anode potentials and therefore resulted in narrower fluctuation as compared with the self-regulated resister scenarios.

3.4. Active harvesting indeed boosted electron transfer and system performance

Table 1 summarizes the average performance data of different reactors operated in various harvesting conditions. It is clear that active harvesting approach significantly increased system output no matter which operational point was desired. For reactors operated at MPP, the MPP-H showed the highest power of 0.38 mW, which was 81% higher than MPP-R and up to 375% higher than other reactors. This is partially reflected by the lower anode potential obtained at MPP reactors. All reactors showed higher than 94% organic removal as brewery wastewater is a easily biodegradable substrate, but the removal rates ranged from 24 to 72 h as shown in Fig. 4. The MCP-H reactor obtained the highest CE of 85± 10% as hypothesized, because higher conversion was gained from organics to current. The MCP-R didn't show higher CE due to the failure of the cathode. The MPP reactors showed lower CE than MCP due to their different operational goal, but MPP-H showed higher CE than MPP-R presumably due to the higher electron transfer rate regulated by the active harvesting circuit. The MVP reactor showed the lowest CE due to the low current. The CV data also confirm that active harvesting increased the biofilm electron transfer activities compared with passive resistors when operated at the same polarization point.

This study demonstrates that the active harvesting approach is very effective in maximizing the performance of MFCs at different operational points. This expands the knowledge from focusing on MPP operation to broader applications of MFCs such as MCP operation for accelerated organic removal, chemical production and desalination. More studies are needed to reveal the potential community structure changes during different operations. Pure culture studies will also be very helpful to elucidate the exact electron transfer mechanism shifts during different harvesting scenarios. While active harvesting showed much higher performance in MFCs, more work on system integration and scale up are needed to realize the potentials for operating practical scale systems.

Table 1
Summary of key results obtained in this study.

Scenario	Power (mW)	Anode potential (mV)	COD removal (%)	CE (%)
MPP-H	0.38	−390	94 ± 1	60 ± 10
MCP-H	0.19	−277	94 ± 0.5	85 ± 10
MPP-R	0.21	−429	95 ± 1	41 ± 2
MCP-R	0.09	−160	95 ± 3	27 ± 5
MVP-R	0.08	−290	95 ± 2	10 ± 1

Acknowledgement

We thank the financial support from CAPES Scholarship 13688-13-8, the Office of Naval Research (Award N000141310901), and the National Science Foundation (CBET 1510682).

Appendix A. Supplementary data

Supplementary data related to this article can be found at http://dx.doi.org/10.1016/j.jpowsour.2017.03.067.

References

[1] H. Wang, H. Luo, P.H. Fallgren, S. Jin, Z.J. Ren, Bioelectrochemical system platform for sustainable environmental remediation and energy generation, Biotechnol. Adv. 33 (2015) 317–334, http://dx.doi.org/10.1016/j.biotechadv.2015.04.003.
[2] W. Li, H. Yu, Z. He, Environmental Science towards Sustainable Wastewater Treatment by Using Microbial Fuel Cells-centered Technologies, Energy Environ. Sci. 7 (2014) 911–924, http://dx.doi.org/10.1039/c3ee43106a.
[3] A. Dewan, S.U. Ay, M.N. Karim, H. Beyenal, Alternative power sources for remote sensors: a review, J. Power Sources 245 (2014) 129–143, http://dx.doi.org/10.1016/j.jpowsour.2013.06.081. Review.
[4] B. Logan, Exoelectrogenic bacteria that power microbial fuel cells, Nat. Rev. Microbiol. 7 (2009) 375–381 (accessed September 17, 2015), http://www.nature.com/nrmicro/journal/v7/n5/abs/nrmicro2113.html.
[5] J. Winfield, L.D. Chambers, A. Stinchcombe, J. Rossiter, I. Ieropoulos, The power of glove: soft microbial fuel cell for low-power electronics, J. Power Sources 249 (2014) 327–332, http://dx.doi.org/10.1016/j.jpowsour.2013.10.096.
[6] H. Wang, J. Park, Z.J. Ren, Practical energy harvesting for microbial fuel cells: a review, Environ. Sci. Technol. 49 (2015) 3267–3277, http://dx.doi.org/10.1021/es5047765.
[7] Y. Kim, M.C. Hatzell, A.J. Hutchinson, B.E. Logan, Capturing power at higher voltages from arrays of microbial fuel cells without voltage reversal, Energy Environ. Sci. 4 (2011) 4662, http://dx.doi.org/10.1039/c1ee02451e.
[8] J. Do Park, Z. Ren, Hysteresis-controller-based energy harvesting scheme for microbial fuel cells with parallel operation capability, IEEE Trans. Energy Convers. 27 (2012) 715–724, http://dx.doi.org/10.1109/TEC.2012.2196044.
[9] M. Alaraj, Z.J. Ren, J.-D. Park, Microbial fuel cell energy harvesting using synchronous flyback converter, J. Power Sources 247 (2014) 636–642, http://dx.doi.org/10.1016/j.jpowsour.2013.09.017.
[10] W. He, J. Liu, D. Li, H. Wang, Y. Qu, X. Wang, et al., The electrochemical behavior of three air cathodes for microbial electrochemical system (MES) under meter scale water pressure, J. Power Sources 267 (2014) 219–226, http://dx.doi.org/10.1016/j.jpowsour.2014.05.028.
[11] H. Wang, Z. Ren, J.-D. Park, Power electronic converters for microbial fuel cell energy extraction: effects of inductance, duty ratio, and switching frequency, J. Power Sources 220 (2012) 89–94, http://dx.doi.org/10.1016/j.jpowsour.2012.07.092.
[12] N. Degrenne, F. Buret, B. Allard, P. Bevilacqua, Electrical energy generation from a large number of microbial fuel cells operating at maximum power point electrical load, J. Power Sources 205 (2012) 188–193, http://dx.doi.org/10.1016/j.jpowsour.2012.01.082.
[13] R.P. Pinto, B. Srinivasan, S.R. Uiot, B. Tartakovsky, The effect of real-time external resistance optimization on microbial fuel cell performance, Water Res. 45 (2011) 1571–1578, http://dx.doi.org/10.1016/j.watres.2010.11.033.
[14] C. Erbay, S. Carreon-Bautista, E. Sanchez-Sinencio, A. Han, High performance monolithic power management system with dynamic maximum power point tracking for microbial fuel cells, Environ. Sci. Technol. 48 (2014) 13992–13999, http://dx.doi.org/10.1021/es501426j.
[15] J.-D. Park, Z. Ren, Hysteresis controller based maximum power point tracking energy harvesting system for microbial fuel cells, J. Power Sources 205 (2012) 151–156, http://dx.doi.org/10.1016/j.jpowsour.2012.01.053.
[16] H. Wang, J.-D. Park, Z. Ren, Active energy harvesting from microbial fuel cells at the maximum power point without using resistors, Environ. Sci. Technol. 46 (2012) 5247–5252, http://dx.doi.org/10.1021/es300313d.

[17] L. Lu, Z.J. Ren, Microbial electrolysis cells for waste biorefinery: a state of the art review, Bioresour. Technol. 215 (2016) 254–264, http://dx.doi.org/10.1016/j.biortech.2016.03.034.
[18] K.S. Jacobson, D.M. Drew, Z. He, Use of a liter-scale microbial desalination cell as a platform to study bioelectrochemical desalination with salt solution or artificial seawater, Environ. Sci. Technol. 45 (2011) 4652–4657, http://dx.doi.org/10.1021/es200127p.
[19] Z. Ren, H. Yan, W. Wang, M.M. Mench, J.M. Regan, Characterization of microbial fuel cells at microbially and electrochemically meaningful time scales, Environ. Sci. Technol. 45 (2011) 2435–2441, http://dx.doi.org/10.1021/es103115a.
[20] D.Y. Lyon, F. Buret, T.M. Vogel, J.M. Monier, Is resistance futile? Changing external resistance does not improve microbial fuel cell performance, Bioelectrochemistry 78 (2010) 2–7, http://dx.doi.org/10.1016/j.bioelechem.2009.09.001.
[21] S. Cheng, H. Liu, B.E. Logan, Increased performance of single-chamber microbial fuel cells using an improved cathode structure, Electrochem. Commun. 8 (2006) 489–494, http://dx.doi.org/10.1016/j.elecom.2006.01.010.
[22] L. Lu, H. Yazdi, S. Jin, Y. Zuo, P.H. Fallgren, Z.J. Ren, Enhanced bioremediation of hydrocarbon-contaminated soil using pilot-scale bioelectrochemical systems, J. Hazard. Mater. 274 (2014) 8–15, http://dx.doi.org/10.1016/j.jhazmat.2014.03.060.
[23] L. Lu, D. Hou, Y. Fang, Y. Huang, Z.J. Ren, Nickel based catalysts for highly efficient H2 evolution from wastewater in microbial electrolysis cells, Electrochim. Acta 206 (2016) 381–387, http://dx.doi.org/10.1016/j.electacta.2016.04.167.
[24] X. Wang, L. Zhou, L. Lu, F.L. Lobo, N. Li, H. Wang, et al., Alternating current influences anaerobic electroactive biofilm activity, Environ. Sci. Technol. 50 (2016) 9169–9176, http://dx.doi.org/10.1021/acs.est.6b00813.
[25] B.E. Logan, B. Hamelers, R. Rozendal, U. Schroder, Microbial fuel Cells;: methodology and technology, Environ. Sci. Technol. 40 (2006) 5181–5192.
[26] W. Wang, P.E. Jenkins, Z. Ren, Electrochemical corrosion of carbon steel exposed to biodiesel/simulated seawater mixture, Corr. Sci. 57 (2012) 215–219, http://dx.doi.org/10.1016/j.corsci.2011.12.015.
[27] W. Zhi, Z. Ge, Z. He, H. Zhang, Methods for understanding microbial community structures and functions in microbial fuel cells: a review, Bioresour. Technol. 171 (2014) 461–468, http://dx.doi.org/10.1016/j.biortech.2014.08.096.
[28] H. Yazdi, L. Alzate-Gaviria, Z.J. Ren, Pluggable microbial fuel cell stacks for septic wastewater treatment and electricity production, Bioresour. Technol. 180 (2015) 258–263, http://dx.doi.org/10.1016/j.biortech.2014.12.100.
[29] Y. Hong, D.F. Call, C.M. Werner, B.E. Logan, Adaptation to high current using low external resistances eliminates power overshoot in microbial fuel cells, Biosens. Bioelectron. 28 (2011) 71–76, http://dx.doi.org/10.1016/j.bios.2011.06.045.
[30] A.S. Commault, G. Lear, M.A. Packer, R.J. Weld, Influence of anode potentials on selection of Geobacter strains in microbial electrolysis cells, Bioresour. Technol. 139 (2013) 226–234, http://dx.doi.org/10.1016/j.biortech.2013.04.047.